CrystEngComm

Accepted Manuscript

ROYAL SOCIETY OF CHEMISTRY

www.rsc.org/crystengcomm

Single crystal structure analysis via magnetically oriented microcrystal arrays

Fumiko Kimura,[a] Wataru Ohshima,[a] Hiroko Matsumoto,[a] Hidehiro Uekusa,[b] Kazuaki Aburaya,[c] Masataka Maeyama[c] and Tsunehisa Kimura*[a]

Received (in XXX, XXX) Xth XXXXXXXXX 20XX, Accepted Xth XXXXXXXXX 20XX
DOI: 10.1039/b000000x

X-ray single crystal structure analysis was performed on three-dimensionally magnetically oriented microcrystal arrays (3D-MOMA) of L-alanine, 1,3,5-triphenyl benzene, and cellobiose. A 3D-MOMA is a composite in which powdery microcrystals are aligned three dimensionally. Microcrystals suspended in UV-curable monomer were subjected to a time dependent magnetic field, followed by consolidation of the monomer to fix the 3D alignment of the microcrystals. The structures determined from X-ray diffracrometry of the three 3D-MOMAs were in excellent agreement with those of the corresponding single crystals reported in literature, demonstrating the usefulness of the 3D-MOMA technique for single crystal structure analyses in circumstances where a large single crystal is not available.

1. Introduction

A single crystal larger than ca. 100 μm in size is usually required for single crystal measurements by a conventional X-ray diffractometer for structure analysis. Furthermore, much larger crystals are necessary for neutron diffraction measurements. However, it is sometimes difficult to obtain crystals large enough for these measurements. Recently, we developed a novel technique to fabricate a three-dimensionally magnetically oriented microcrystal array (3D-MOMA) suitable for single crystal diffraction experiments. A 3D-MOMA is a composite in which microcrystals are aligned three-dimensionally in a polymer matrix. The X-ray diffraction of the MOMA is equivalent to that of the corresponding large single crystal, enabling the determination of the crystal structure of the embedded microcrystals.

The 3D-MOMA technique can be applied to biaxial crystals (orthorhombic, monoclinic, and triclinic crystal systems), whose magnetic susceptibility tensor has three different principal values, χ_1, χ_2, and χ_3 (defined as $\chi_1 > \chi_2 > \chi_3$). Under a static magnetic field, the easy magnetization axis χ_1 aligns parallel to the applied magnetic field, while under a rotating magnetic field, the hard magnetization axis χ_3 aligns perpendicular to the plane of the field rotation. Application of a combined static and rotating (referred to as time-dependent) magnetic field produces 3D alignment (that is, biaxial alignment of χ_1 and χ_3 axes) of microcrystals.[1-5] The achieved alignment is fixed by cure of suspending liquid matrix to obtain a 3D-MOMA.

We already prepared 3D-MOMAs of $LiCoPO_4$[6] (orthorhombic *Pnma*) sucrose[7] (monoclinic $P2_1$) and lysozyme[8] (orthorhombic $P2_12_12_1$) and showed that they can produce X-ray diffraction needed to perform single crystal analyses using conventional software. The determined crystal structures were in excellent agreement with those for the corresponding single crystals reported in literatures.[9-10]

The quality of 3D-MOMA depends on various factors including point group and the degree of anisotropic magnetic susceptibility of crystal, choice of applied time-dependent magnetic field, etc. However, these factors have not been fully examined. In this paper, we chose L-alanine (orthorhombic $P2_12_12_1$), 1,3,5-triphenylbenzene (TPB: orthorhombic $Pna2_1$), and cellobiose (monoclinic $P2_1$) to evaluate the effects of these relevant factors. Furthermore, the crystal structures of these crystals are solved using their 3D-MOMA samples and compared with those for corresponding single crystals reported in literatures.

2. Experimental

2.1 Preparation of microcrystal suspension

L-alanine, TPB, sodium dodecyl sulphate (SDS), and polyethylene glycol 400 were purchased from Wako Pure Chemical Industries, Ltd., and used without further purification. Cellobiose was generously donated by Matsutani Chemical Industry Co., Ltd. and used as-received.

About 0.5 g L-alanine crystal was pulverized using a mortar and mixed with ca. 0.1 ml 0.25% acetone solution of SDS, and dispersed in a UV-curable monomer (No. 8815 of Kyoritsu Chemical and Co. Ltd., viscosity of 1.2 Pa s) to obtain a microcrystalline suspension. The concentration of the microcrystallites was ca. 10 wt%.

About 0.15 g TPB was pulverized with a mortar and ca. 250 μL of polyethylene glycol 400 was added. Next, the TPB powder was mixed with UV curable monomer (BEAMSET 550DC of Arakawa Chemical Industries, Ltd., viscosity of 2.0 Pa s) to produce a suspension. TPB concentration was ca. 15 wt%.

About 0.8 g cellobiose was pulverised with a mortar and mixed with UV curable monomer (XVL-14 of Kyoritsu Chemical and Co. Ltd., viscosity of 12 Pa s) to prepare a suspension.

2.2 Non-uniform sample rotation in a static magnetic field

About 0.1 ml of each of suspensions was taken and poured into a plastic container. The container was mounted on a sample-rotating stage and subjected to a horizontal static magnetic field generated by a superconducting magnet (**Fig. 1**).[11] The suspension was rotated non-uniformly in the applied field for 2 h (L-alanine), 5 min (TPB), and 1 h (cellobiose), respectively, and was then exposed to UV-light to cure the matrix and fix the

alignment. Each suspension was rotated at a non-uniform angular velocity in the horizontal magnetic field. The rotation axis was vertical. The intensities of the magnetic field were 5 T for L-alanine, 2 T for TPB, and 8 T for cellobiose. The rotation speed was switched between ω_s and ω_q ($\omega_s < \omega_q$) every 90 degree. These velocities were: ω_s = 5 and ω_q = 25 rpm for L-alanine, ω_s = 20 and ω_q = 100 rpm for TPB, and ω_s = 10 and ω_q = 80 rpm for cellobiose. (Sample rotation in a static magnetic field is equivalent to application of a rotating magnetic field to a still sample.) The χ_3 axis aligns parallel to the sample rotation axis and the χ_1 axis aligns in the direction of the longest duration of the magnetic field.

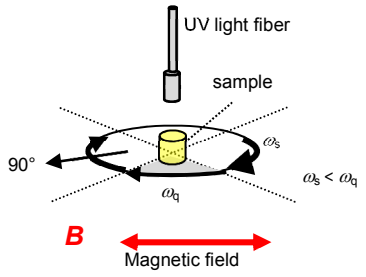

Fig. 1 Modulated sample rotation to generate modulated magnetic field.

2.3 X-ray structure analysis

Each of 3D-MOMAs was cut into a specimen ~ 0.9 × 0.8 × 0.8 mm (for L-alanine), ~ 0.1 × 0.1 × 0.1 mm (for TPB) and ~1.0 × 1.0 × 1.1 mm (for cellobiose), then mounted on a glass fibre for X-ray measurement. All the measurements were performed using a Rigaku R-AXIS RAPID diffractometer equipped with an imaging-plate area detector using graphite-monochromated Cu Kα radiation, at 293 K, 296 K, and 296 K, for L-alanine, TPB, and cellobiose, respectively. Collimator size was 0.8 mm in diameter. The structure was solved by direct methods and expanded using Fourier techniques.

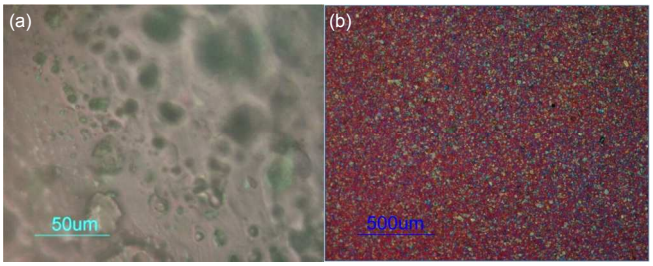

Fig. 2 Polarized optical micrographs of (a): TPB MOMA and (b): cellobiose suspension.

3. Results and Discussion

3.1 Crystal structure analysis using MOMA

An optical micrograph of the TPB MOMA is in **Fig. 2(a)**. The microcrystals are up to 50 μm in size. **Fig. 2(b)** is an optical micrograph of the cellobiose suspension. Microcrystals were up to 25 μm in size and their dispersion was excellent.

Typical diffraction images obtained from the MOMAs of L-alanine, TPB, and cellobiose are in **Fig. 3(a), (b), and (c)**, respectively. The MOMAs of L-alanine and cellobiose exhibit diffraction spots at larger 2θ values, while TPB MOMA exhibits diffraction spots only at smaller 2θ values.

The crystal system of L-alanine determined from the 3D-MOMA is primitive orthorhombic and the lattice parameters are a = 5.7837(3), b = 6.0328(3), c = 12.3406(6) Å, V = 430.59(4) Å^3, and Z = 4. The space group is $P2_12_12_1$ (#19). The R_1 and wR_2 values are 0.0662 and 0.1718, respectively, as summarized in **Table 1**. These values are about two times larger than the values reported for the single crystal.[12)]

The lattice parameters of TPB, which has a primitive orthorhombic unit cell, are a = 7.5958(2), b = 19.7480(14), c = 11.2510(3) Å, V = 1687.68(13) Å^3 and Z = 4. The space group is $Pna2_1$ (#33). The R_1 and wR_2 values are 0.0993 and 0.3082, respectively (**Table 1**). The R_1 and wR_2 values are larger than that of the L-alanine MOMA because diffraction spots were not observed at larger 2θ areas. In terms of the half width of diffraction spots, the alignment of the TPB microcrystals is as good as that of the L-alanine microcrystals. Therefore, less spots

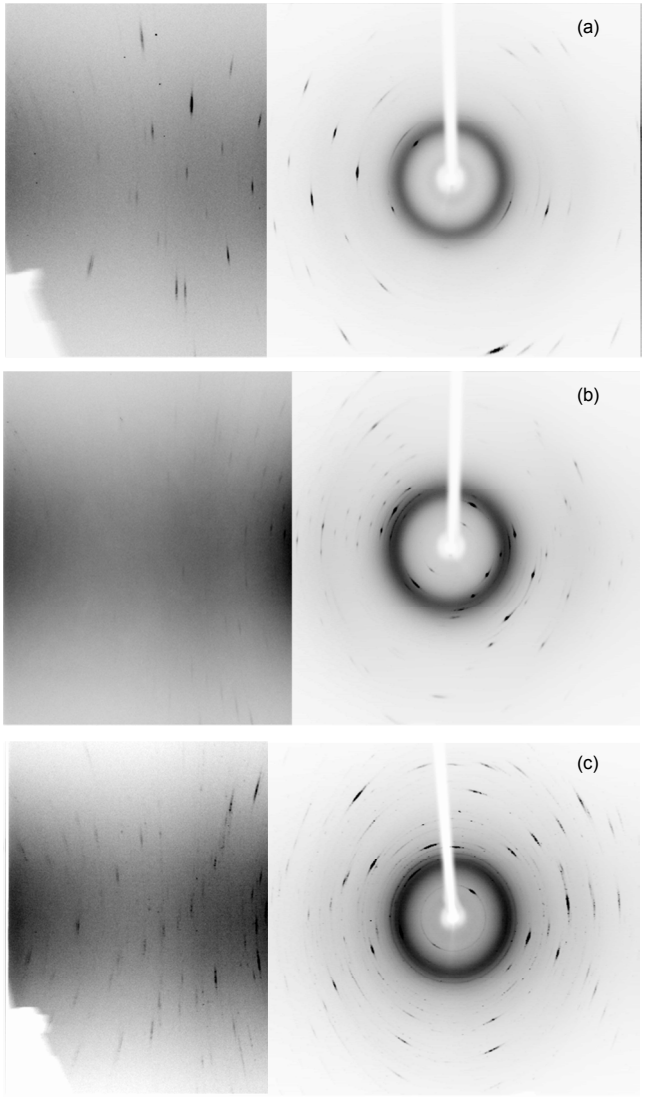

Fig. 3 Diffraction images obtained from MOMAs of (a) L-alanine, (b) TPB, and (c) cellobiose. Contrasts are different between left and right halves.

Table 1 Crystal graphic data obtained from MOMA and single crystals.

sample	L-alanine MOMA	L-alanine	TPB MOMA	TPB	cellobioseMOMA	cellobiose
crystal system	orthrombic	orthorhombic	orthorhombic	orthorhombic	monoclinic	monoclinic
space group	$P2_12_12_1$	$P2_12_12_1$	$Pna\,2_1$	$Pna\,2_1$	$P2_1$	$P2_1$
temperature	293.1	295(2)	296	293	296	173.0(1)
a (Å)	5.7837(3)	5.7762(9)	7.5958(2)	7.620(1)	5.0868(3)	5.0633(2)
b (Å)	6.0328(3)	6.0345(10)	19.7480(14)	11.265(1)	13.0628(8)	13.0170(5)
c (Å)	12.3406(6)	12.361(3)	11.2510(3)	19.772(5)	10.9758(7)	10.9499(4)
α (°)	90.0000	90.00	90.0000	90.00	90.0000	90.000
β (°)	90.0000	90.00	90.0000	90.00	90.990(7)	90.811(2)
γ (°)	90.0000	90.00	90.0000	90.00	90.0000	90.000
V (Å^3)	430.59(4)	430.86(14)	1687.68(13)	1697.349	729.21(8)	721.62(5)
Z	4	4	4	4	2	2
θ_{max} (X-ray source)	68.2 (Cu)	26.37 (Mo)	136.4 (Cu)	24.99(Mo)	68.25 (Cu)	27.103 (Mo)
R_1	0.0662	0.0378	0.0993	0.0397	0.1062	0.0391
wR_2 [all data]	0.1718	0.0754	0.3082	0.909	0.3323	0.0841
GOF	1.018	1.044	1.031	1.000	1.146	1.049
CCDC No.	970543	756484	970545	867818	970544	673203

$R_1 = \Sigma\,||Fo| - |Fc||\,/\,\Sigma\,|Fo|$, $wR_2 = [\,\Sigma\,(\,w\,(Fo^2 - Fc^2)^2)/\,\Sigma\,w(Fo^2)^2]^{1/2}$

at larger 2θ areas for TPB is probably due to low crystallinity of the original microcrystalline TPB.

In general, the principal axes χ_1, χ_2, and χ_3 of the susceptibility tensor of biaxial crystals do not necessarily coincide with the crystallographic axes. However, the *b*-axis (two-fold axis) of monoclinic system coincides with one of the three susceptibility axes. Since these three axes are mutually perpendicular, the other two axes are located in the *ac* plane.[13] The monoclinic system includes three point groups, that is, 2, *m*, and 2/*m*. In 2 and 2/*m*, the π-rotation about the susceptibility axes can produce a new orientation. Because of the two-fold symmetry of magnetic field, this new orientation has the same magnetic energy, occurring at the same probability. As a result, their 3D-MOMAs are a mixture of these two orientations. On the other hand, in *m*, the π-rotation about the three susceptibility axes can produce three new orientations. Therefore, its 3D-MOMA is a mixture of four orientations.

Because the cellobiose crystal belongs to the point group (2), there are two orientations in its 3D-MOMA.[7] These two orientations produce a diffraction pattern similar to that produced by a twin crystal. Therefore, using software designed for the analysis of the twin structure, the diffraction image of the cellobiose 3D-MOMA was analysed. The lattice parameters for this primitive monoclinic unit cell are a = 5.0868(3) Å, b = 13.0628(8) Å, c = 10.9758(7) Å, β = 90.990(7) Å , V = 729.21(8) Å^3, and Z = 2. The space group is $P2_1$ (No. 4).

The two-fold axis (*b* axis) of cellobiose coincides with one of the magnetic susceptibility axes, χ_1, χ_2, or χ_3, as described previously. It is reported in our previous work[14] that χ_3 corresponds to the *b* axis. Since the three magnetic susceptibility axes are mutually perpendicular, the other two axes χ_1 and χ_2, are located in the *ac* plane. However, there is no general rule to relate these magnetic susceptibility axes to the *a* and *c* axes.[13] The twin structure was solved as shown in **Fig. 4**. The magnetic susceptibility axes are also shown. Twin matrix TM was determined as follows.

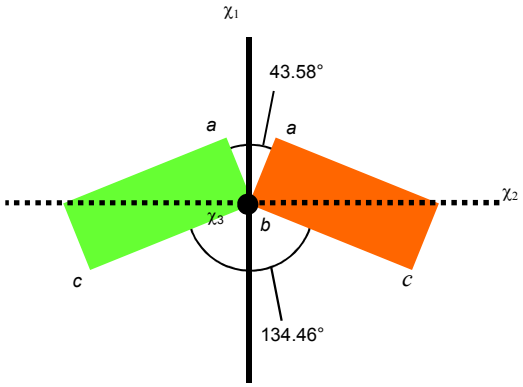

Fig. 4 Twin structure of a 3D-MOMA of cellobiose. The *b* axis and the hard magnetization axis χ_3 are placed perpendicular to the plane of the diagram. The other axes, χ_1 and χ_2, are placed in the plane. The angle between the *a* axis and the χ_1 axis is 21.8°.

$$\mathrm{TM} = \begin{pmatrix} 0.6231 & -0.7795 & 0.0640 \\ -0.7795 & -0.6256 & -0.0303 \\ 0.0637 & -0.0310 & -0.9975 \end{pmatrix}$$

The direction of the longest exposure time to the magnetic fields in the sample corresponds to the χ_1 axis which can be roughly determined from the experimental setting of the sample under the magnetic field and the direction parallel to the rotating axis corresponding to the χ_3 axis also can be determined using the sample setting. The angle between the χ_1 axis and the *a* axis is determined to be 21.79°. This result is consistent with our previous result[14], in which the angle was determined using one-dimensional MOMAs (alignments under a static and a rotating magnetic field). The R_1 and wR_2 were 0.1062 and 0.3323, respectively (cf. **Table 1**).

Our present results, alongside those from the literature,[12,15,16]

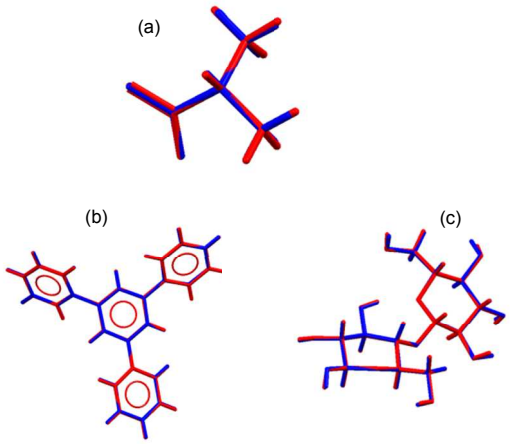

Fig. 5 Comparison of the structures determined in this study (blue) and the structure reported previously (red).
(a): L-alanine (RMSD=0.0055 Å), (b): TPB (RMSD=0.0214 Å), (c): cellobiose (RMSD=0.0189 Å).

are shown graphically in **Fig. 5**. The atomic coordinates determined in this study are in excellent agreement with those determined using a traditional single crystal.

3.2 Anisotropic fluctuations of microcrystals

There are many kinds of time-dependent magnetic fields.[1-5] In the case of frequency-modulated elliptical magnetic field (the speed of rotation changes between ω_s and ω_q every 90° **(Fig. 1)**, which we used in this study), the fluctuations in orientation about each of the χ_1, χ_2, and χ_3 axes, $<\Delta\psi^2>^{1/2}$, $<\Delta\theta^2>^{1/2}$, and $<\Delta\phi^2>^{1/2}$, respectively, are different in amplitude.[3,17] The fluctuation $<\Delta\theta^2>^{1/2}$ is the smallest because the magnetic anisotropy χ_1-χ_3 is the largest by definition ($\chi_1>\chi_2>\chi_3$). The square intensities of the fluctuations about the χ_1, χ_2, and χ_3 axes are derived from our previous work[17] expressed by the following equations:

$$< \Delta\psi^2 >= C \frac{2\,(r_\omega + 1)}{(\chi_2 - \chi_3)((-2+\pi)\,r_\omega + (2+\pi))} \quad \text{----(1)}$$

$$< \Delta\theta^2 >= C \frac{2\,(r_\omega + 1)}{(\chi_1 - \chi_3)((2+\pi)\,r_\omega + (-2+\pi))} \quad \text{---(2)}$$

$$< \Delta\phi^2 >= C \frac{(r_\omega + 1)}{2\,(\chi_1 - \chi_2)(r_\omega - 1)} \quad \text{----------(3)}$$

where $C = \pi k_B T \mu_0 / B^2 V$ and r_ω is the ratio ω_q/ω_s.

Fig. 6 shows the theoretical r_ω-dependence of the fluctuations for L-alanine[18] and TPB[19]. The values used for calculation are in **Table 2**. Though $<\Delta\theta^2>^{1/2}$ is strictly the smallest over the whole range of r_ω, $<\Delta\psi^2>^{1/2}$ and $<\Delta\phi^2>^{1/2}$ can be equal at a certain value of r_ω. Equalizing these components is favourable to obtaining well-resolved diffraction patterns. The equalization is achieved at r_ω=3.7 for L-alanine. On the other hand, there is not an equalization condition for the TPB 3D-MOMA because values of χ_1 and χ_2 are very close. However, its fluctuation level is almost the same as that of L-alanine, and hence the equalization is not an important factor for the TPB MOMA in the present case.

The magnetic anisotropy of TPB (χ_1- χ_2= 0.68×10^{-6} and χ_2- χ_3= 7.53×10^{-6}) is larger than that of L-alanine (χ_1- χ_2=2.6×10^{-7} and χ_2- χ_3=3.0×10^{-7}). This might explain the fact that the intensity of the fluctuations of the TPB MOMA is almost the same as that of the L-alanine MOMA in spite of the fact that value of the applied magnetic field for the TPB sample is 2.5 times smaller than that for the L-alanine sample.

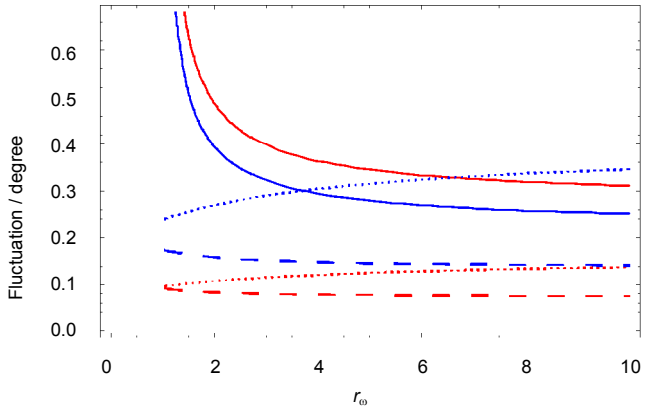

Figs. 6 Fluctuations of $<\Delta\psi^2>^{1/2}$, $<\Delta\theta^2>^{1/2}$, and $<\Delta\phi^2>^{1/2}$ as a function of r_ω. Blue lines are for L-alanine and red lines are for TPB. Solid, dotted, and broken lines correspond to the fluctuation of $<\Delta\phi^2>^{1/2}$, $<\Delta\psi^2>^{1/2}$, and $<\Delta\theta^2>^{1/2}$, respectively. The values used for calculation are summarized in Table 2.

Table 2 Values used for calculation of fluctuation and observed fluctuation

3D-MOMA	L-alanine	TPB
magnetic field /T	5	2
χ_1	-9.84×10^{-6} [18]	-6.99×10^{-6} [19]
χ_2	-10.1×10^{-6} [18]	-7.67×10^{-6} [19]
χ_3	-10.4×10^{-6} [18]	-15.2×10^{-6} [19]
V (μm^3) used for calculation	80×10^{-18}	125×10^{-18}
$\Delta\phi$ /degree	0.23	0.35
$\Delta\varphi$ /degree	0.35	0.013
$\Delta\theta$ /degree	0.14	0.008
Observed average fluctuation /degree	2.8-3.5	2.0-3.6

Table 2 shows that calculated fluctuation values are less than 1.0 degree. However, experimental values range between 2 and 4 degrees, which are about ten times larger than calculated values. The difference can be attributed to the deterioration of orientation during the process of 3D alignment consolidation. If a magnetically oriented microcrystal suspension (MOMS) is used instead of a MOMA, narrower diffraction spots are obtained.[20]

4. Conclusions

Three dimensionally magnetically oriented microcrystal arrays (3D-MOMAs) prepared from microcrystalline powders of L-alanine, 1,3,5-triphenyl benzene, and cellobiose were fabricated using the time-dependent magnetic field. The 3D-MOMAs exhibited well-resolved diffraction spots, indicating sufficient diffracted signal for structure analysis. The structures determined in this study are in excellent agreement with those determined by

using the corresponding single crystals reported in literature. The technique presented here provides a facile approach to the single crystal analysis when only a microcrystalline powder is available.

Acknowledgment This research was partially supported by the Ministry of Education, Culture, Sports, Science and Technology (24350119). Computation time was provided by the SuperComputer System, Institute for Chemical Research, Kyoto University.

Notes and references

[a] *Division of Forest and Biomaterials Science, Kyoto University, Sakyo-ku, Kyoto 606-8502, Japan. Tel: +81-75-753-6246; Fax: +81-75-753-6300; E-mail: tkimura@kais.kyoto-u.ac.jp*
[b] *Department of Chemistry and Materials Science, Tokyo Institute of Technology, Ookayama 2, Meguro-ku, Tokyo 152-8551, Japan*
[c] *Rigaku Corporation, 3-9-12 Matsubara-cho, Akishima, Tokyo 196-8666, Japan*

† Electronic Supplementary Information (ESI) available: [details of any supplementary information available should be included here]. See DOI: 10.1039/b000000x/

1 T. Kimura and M. Yoshino, *Langmuir* 2005, **21**, 4805.
2 M. Staines, J.-Y. Genoud, A. Mawdsley and V. K. Manojlovic, *IEEE Trans. Appl. Supercond.*, 1999, **9**, 5584.
3 M. Yamaguchi, S. Ozawa, I. Yamamoto and T. Kimura, *Jpn. J. Appl. Phys.*, 2013, **52**, 013003.
4 N. Nakatsuka, H. Yasuda, T. Nagira and M. Yoshiya, J. Phys.: Conf. Ser., 2009, **165**, 012021.
5 T. Fukushima, S. Horii, H. Ogino, T. Uchikoshi, T. S. Suzuki, Y. Sakka, A. Ishihara, J.-I. Shimoyama and K. Kishio, *Appl. Phys. Exp.*, 2008, **1**, 111701.
6 T. Kimura, C. Chang, F. Kimura and M. Maeyama, *J. Appl. Cryst.*, 2009, **42**, 535.
7 F. Kimura, T. Kimura, W. Oshima, M. Maeyama and K. Aburaya, *J. Appl. Cryst.*, 2010, **43**, 151.
8 F. Kimura, K. Mizutani, B. Mikami and T. Kimura, *Cryst. Growth Des.*, 2011, **11**, 12.
9 F. Z. Kubel, *Z. Kristallogr.*, 1994, **209**, 755.
10 Hanson, J. C., Sieker, L. C. & Jensen, L. H. (1973). *Acta Cryst. B, **29***, 797.
11 F. Kimura, T. Kimura, K. Matsumoto, and N. Metoki, *Cryst. Growth Des.*, 2010, **10**, 48.
12 V. S. Mom'Kov, Yu. A. Chesalov and E. V. Bildyreva, *Zh. Struct. Kheim.*, 2010, **51**, 1091.
13 J. F. Nye (1985). Physical Properties of Crystals, ch. 3. Oxford: Clarendon Press.
14 G. Song, K. Matsumoto, K. Fujita, F. Kimura and T. Kimura, *J. J. Applied Physics*, 2012, **51**, 060203.
15 D. Prasad, A. Preetam, M. Nath, *Comptes Rendus Chimie*, 2013, **16**, 252.
16 E. Kaenius, T. Kekalainen, R. Neitola, K. Rissanen and P. Vainiotalo, *Chem. – Eur. J.*, 2008, **14**, 5220.
17 T. Kimura, T. Tanaka, G. Song, K. Matsumoto, K. Fujita and F. Kimura, *Cryst. Growth Des.*, 2013, **13**, 1815.
18 K. Ogawa, Thesis, Iwate University (2005).
19 R. R. Gupta: in Landolt-Bornstein, ed. H.-H. Hellwege and A. W. Hellwege (Springer, Berlin, 1986) Vol. II/16, Chap. 8.
20 K. Matsumoto, F. Kimura, S. Tsukui and T. Kimura, *Cryst. Growth Des.* 2011, **11**, 945.

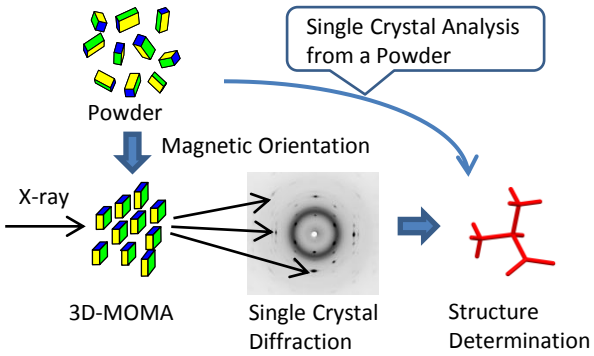

Single crystal structure determination is possible from a powder sample without preparing a large single crystal.